Applied Physics Letters

RESEARCH ARTICLE | JULY 30 2025

Wide bandgap perovskite photovoltaic on rigid and flexible substrates for indoor light harvesting

Ram Datt ; Jinyan Guo ; Renxing Lin ; Ludong Li ; Hairen Tan ; Wing Chung Tsoi

Appl. Phys. Lett. 127, 043903 (2025)
https://doi.org/10.1063/5.0284313

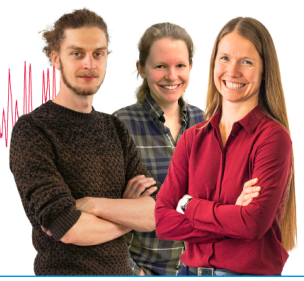

AIP Publishing

Applied Physics Letters ARTICLE pubs.aip.org/aip/apl

Wide bandgap perovskite photovoltaic on rigid and flexible substrates for indoor light harvesting

Cite as: Appl. Phys. Lett. **127**, 043903 (2025); doi: 10.1063/5.0284313
Submitted: 6 June 2025 · Accepted: 14 July 2025 ·
Published Online: 30 July 2025

Ram Datt,[1] Jinyan Guo,[2] Renxing Lin,[2] Ludong Li,[2,a)] Hairen Tan,[2] and Wing Chung Tsoi[1,a)]

AFFILIATIONS

[1]SPECIFIC, Faculty of Science and Engineering, Swansea University, Bay Campus, Fabian Way, Swansea SA1 8EN, United Kingdom
[2]National Laboratory of Solid State Microstructures, Collaborative Innovation Center of Advanced Microstructures, College of Engineering and Applied Sciences, Frontiers Science Center for Critical Earth Material Cycling, Nanjing University, Nanjing 210023, China

Note: This paper is part of the Special Topic, High-Performance Thin-Film Indoor Photovoltaics.
[a)]**Authors to whom correspondence should be addressed:** ludongli@nju.edu.cn and w.c.tsoi@swansea.ac.uk

ABSTRACT

Perovskite photovoltaics (PPV), due to their compatibility with a flexible substrate, low cost, and high indoor performance compared to existing inorganic and organic photovoltaic technologies, are emerging as a potential candidate to power the internet of things (IOT). Dual-cation and mixed halide [$FA_{0.8}Cs_{0.2}Pb(I_{0.62}Br_{0.38})_3$] (FACsPbIBr) based wide bandgap perovskite composition's long-term stability and energy bandgap made them ideal for indoor applications. In this work, we have developed the PPV devices using flexible substrate based on FACsPbIBr perovskite composition for indoor application. PPV were also fabricated on rigid substrate as control devices. The flexible and rigid substrate-based PPV devices delivered power conversion efficiency (PCE) of 17.02 (36.33)% and 18.90 (37.25)%, respectively, under AM1.5G (LED 2700 K, 1000 lux). Remarkably, flexible-PPV devices delivered open-circuit voltage (V_{OC}) of 1.11 V under indoor light (1000 lux). The study suggests the potential of flexible substrate-wide bandgap perovskite-based PPV for futuristic IOT applications.

Indoor photovoltaics (IPV) have emerged as a promising energy source to replace or achieve sufficient battery life for powering the internet of things (IOT), an interconnected network of tiny, micropowered electronics devices.[1,2] Among various photovoltaics (PV), perovskite photovoltaics (PPV) have received significant attention due to their exceptional optical and electrical properties, such as tunable bandgap (tune absorption) and high absorption coefficient. Their compatibility with low-cost fabrication methods and flexible substrates also opens new opportunities to easily integrate with ambient electronics and power them in smart homes, offices, and industries.[3–6] With the advancements in the composition of perovskite materials, interface layers, passivation techniques, and device structures over the last decade, the power conversion efficiencies (PCEs) of PPV have been up to 26.1% and 44.70% under AM 1.5G and indoor light illumination, respectively.[7–10] However, the PPV reported with the highest PCE showed a low open-circuit voltage (V_{OC}) under indoor light illumination.[8,11] A higher V_{OC} is advantageous in reducing the number of cells in a module to get required voltage to drive indoor gadgets.[12] A triple-anion $CH_3NH_3PbI_{2-x}BrCl_x$ perovskite PPV delivered PCE of 36.2% with a V_{OC} of 1.02 V under 1000 lux.[13] Zhang *et al.* demonstrated PPV using a series of wide bandgap perovskites ($Cs_{0.17}FA_{0.83}PbI_{3-x}Br_x$) by varying Br contents ($0.6 \leq x \leq 1.6$) and the champion device shown V_{OC} and PCE of 1.05 V and 34.60% under 1000 lux, respectively.[14] Ma *et al.* introduced poly(amidoamine) as a passivation layer, and the device based on the $CsPbI_2Br$ perovskite film has achieved V_{OC} and PCE of 1.06 V and 35.71%, respectively, under 1000 lux.[15] The hybrid halide perovskites ($MAPbI_{3-n}Br_n$) with stoichiometry (n = 0, 1, 2, and 3) reached V_{OC} up to 1.15 V under indoor light, whereas the PCEs were low (19.94%).[16] Li *et al.* and Ma *et al.* demonstrated the highest PCE up to 42.12% and 44.72% under 1000 lux, whereas the devices delivered V_{OC} up to 0.89 and 1.06 V, respectively.[10,17] Research is less focused on achieving both high V_{OC} and high PCE. Flexible-PPV is also necessary for indoor application. Skafi *et al.* presented $Cs_{0.08}(FA_{0.78}MA_{0.16})$ Pb $(I_{0.84}Br_x)_3$ perovskite-based PPV using flexible substrate, and the devices delivered PCE up to 32.5% with the V_{OC} of 0.957 V.[18] The highest PCE and V_{OC} reported for flexible-PPV are 41.33% and 0.979 V, respectively.[19] The research focus needs to be given to achieving high V_{OC} and PCE for flexible-PPV under indoor light illumination.

In this work, we have presented the dual-cation and mixed halide ($FA_{0.8}Cs_{0.2}Pb(I_{0.62}Br_{0.38})_3$) (FACsPbIBr) perovskite-based PPV for

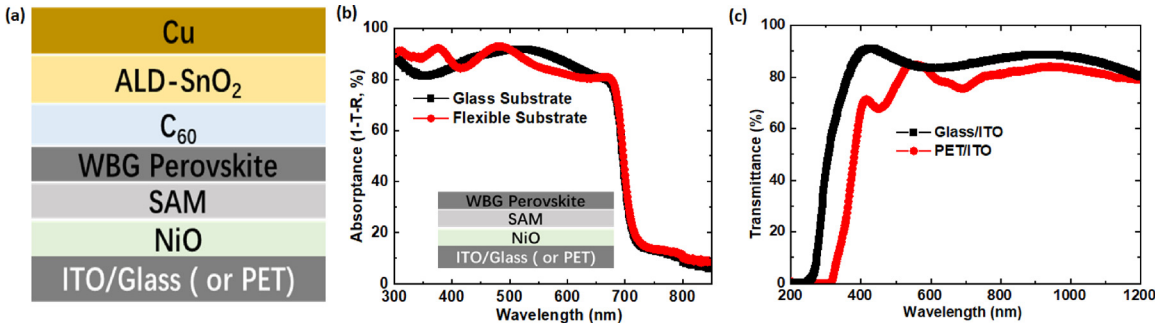

FIG. 1. (a) Device structure, (b) absorptance spectra (measured from substrate side) of perovskite film coated on top of rigid and flexible substrates (inserted the film structure), and (c) transmittance spectra of glass (PET)/ITO substrates.

indoor application, delivering balance between high V_{OC} and PCE (under 1000 lux). The indoor photovoltaic performance of devices fabricated using flexible and rigid substrates has been studied. The light intensity-dependent measurement was also conducted.

The material and device fabrication details are provided in the supplementary material (Sec. 1). For simplicity, the devices fabricated on flexible and rigid substrates are mentioned as flexible-PPV and rigid-PPV, respectively, throughout this paper. Figure 1(a) shows the device structure fabricated on rigid and flexible substrates. The AAA class Newport simulator (Model No: 94023A), equipped with Keithley 2400, was used to measure current density–voltage (J–V) characteristics under AM 1.5G (1 Sun). The light intensity was calibrated using standard reference silicon cell. External quantum efficiency (EQE) was measured using in-house-made systems, and chopper frequency of 71 Hz was used without bias illumination. The indoor measurements were conducted using in-house-made light emitting diode (LED-2700 K, spectrum is shown in Fig. S6) based system, equipped with a 2200 keithley. Optical transmittance, reflectance, and absorptance measurements were carried out in a Lambda 950 ultraviolet-visible spectrophotometer.

Figure 1(b) shows absorptance spectra (transmittance and reflectance spectra are given in the supplementary material, Fig. S1) of film coated on PET/ITO/NiO/SAM/Perovskite (flexible) and glass/ITO/NiO/SAM/Perovskite (glass). The glass-coated perovskite film had higher absorption due to substrate's low transmission loss [Fig. 1(c)]. The energy bandgap calculated (Fig. S2, supplementary material) for perovskite film coated on rigid and flexible substrates was 1.760 and 1.758 eV, respectively. Figures 2(a) and 2(b) show the J–V characteristics (reverse and forward scan) of the flexible and rigid-PPV devices measured under AM1.5G (100 mW/cm^2), and the summary of the device parameters is shown in Table I. The presented outcome is the average of eight devices. Flexible-PPV devices delivered V_{OC}, short-

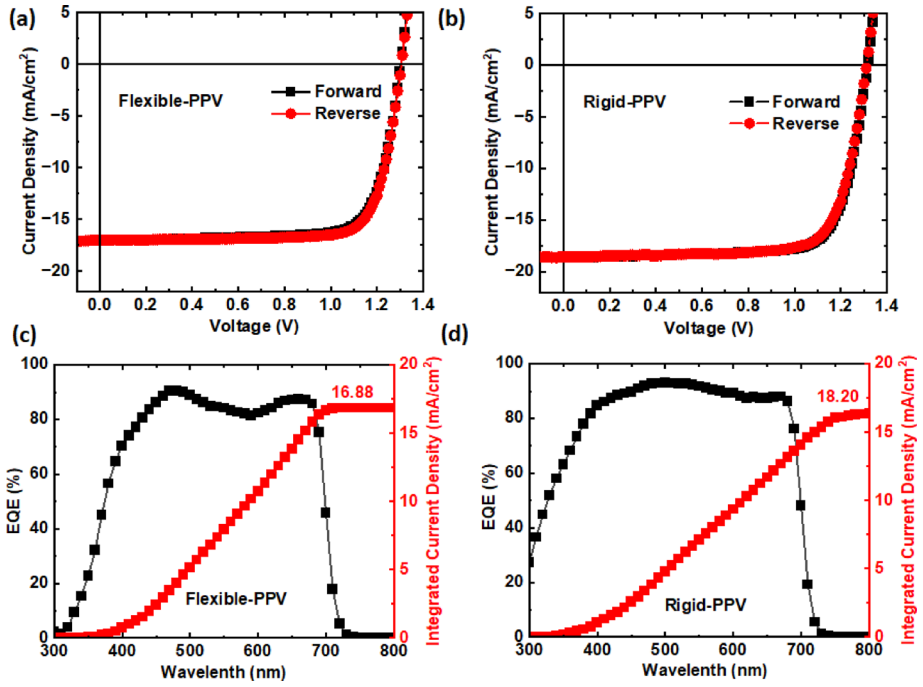

FIG. 2. J–V characteristics (AM 1.5G) of (a) flexible-PPV and (b) rigid-PPV. EQE (AM 1.5G) spectra of (c) flexible-PPV and (d) rigid-PPV.

TABLE I. Device parameters of flexible-PPV and rigid-PPV measured under AM1.5 G (1 Sun).

Device	Scan	V_{OC} (V)	J_{SC} (mA/cm^2)	J_{EQE} (mA/cm^2)	FF (%)	PCE (%)
Flexible-PPV	Forward	1.303	17.10	16.88	77.38	17.02
	Reverse	1.305	17.06		78.44	17.24
Rigid-PPV	Forward	1.317	18.21	18.20	78.75	18.90
	Reverse	1.306	18.04		77.75	18.20

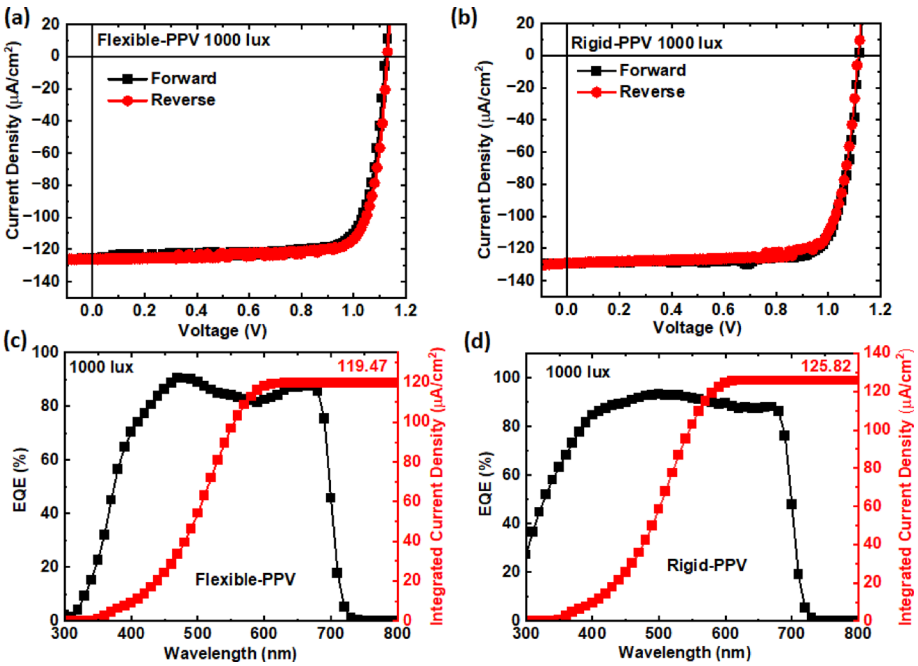

FIG. 3. J–V characteristics (under 1000 lux) of (a) flexible-PPV and (b) rigid-PPV. EQE (1000 lux) spectra of (c) flexible-PPV and (d) rigid-PPV.

circuit current (J_{SC}), fill factor (FF), and PCE of 1.303 V, 17.10 mA/cm^2, 77.38%, and 17.02%, respectively, under forward scan. In reverse scan, the PCE was 17.24%, which shows low hysteresis, whereas rigid-PPV devices delivered V_{OC}, J_{SC}, FF, and PCE of 1.317 V, 18.21 mA/cm^2, 78.75%, and 18.90%, respectively, under forward scan. Devices showed a similar outcome in reverse scan (PCE ∼ 18.20%), which shows low hysteresis. In both devices, the integrated current density (J_{EQE}) calculated using EQE was under 5% differences from J_{SC}, as shown by the EQE plots in Figs. 2(c) and 2(d). The lower PCE (∼17.02%) of flexible-PPV than that of rigid-PPV (∼18.90%) is mainly due to the lower transmittance of flexible substrates (compared to glass substrates) [Fig. 1(c)] which leads to lower J_{SC} and causes low performance.

The indoor performance of the flexible-PPV and rigid-PPV devices was measured using a 2700 K LED under 1000 lux. Figures 3(a) and 3(b) show J–V characteristic of flexible and rigid-PPV measured under 1000 lux, and the summary of the devices is shown in Table II. Flexible-PPV devices showed V_{OC}, J_{SC}, FF, and PCE of 1.117 V, 125.59 μA/cm^2, 80.22%, and 36.33%, respectively, measured under 1000 lux. The devices show low hysteresis [Fig. 3(a)] measured in forward and reverse scan under 1000 lux illumination. Rigid-PPV devices delivered V_{OC}, J_{SC}, FF, and PCE of 1.111 V, 129.29 μA/cm^2, 80.33%, and 37.25% under 1000 lux (forward scan). The devices show low hysteresis in forward and reverse scan under 1000 lux [Fig. 3(b)]. Indoor measurement's reliability depends on the closeness of J_{SC} with J_{EQE} calculated using 1000 lux illumination spectrum. Flexible and rigid-PPV

TABLE II. Device parameters of flexible-PPV and rigid-PPV measured under indoor lights (1000 lux).

Device	Scan	V_{OC} (V)	J_{SC} (μA/cm^2)	J_{EQE} (μA/cm^2)	FF (%)	PCE (%)
Flexible-PPV	Forward	1.117	125.59	119.47	80.22	36.33
	Reverse	1.116	125.98		79.89	36.26
Rigid-PPV	Forward	1.111	129.29	125.82	80.33	37.25
	Reverse	1.107	129.15		79.95	36.93

TABLE III. A summary of reported high performance PPV (flexible) for indoor applications.

Illumination (lux)	Perovskite	Bandgap (eV)	V_{oc} (V)	J_{sc} (μA/cm^2)	FF (%)	PCE (%)	Reference
1000	$(FAPbI_3)_{0.85}$ $(MAPbBr_3)_{0.15}$	1.61	0.80	120	69	17.7	20
LED, 6400 K, 1000	$MAPbI_3/FAPbIBr_2 = 0.95{:}0.05$)	⋯	0.967	251	73.3	25.74	21
LED, 1000	$Cs_{0.08}(FA_{0.78}$ $MA_{0.16})$ Pb $(I_{0.84}Brx)_3$	1.63	0.957	172	77.7	32.5	18
LED, 3000 K, 1000	Perovskite	1.52	0.979	139.7	84.32	41.33	19
LED, 3000 K, 1000	$FA_{0.8}Cs_{0.2}Pb$ $(I_{0.62}Br_{0.38})_3$	1.76	1.117	125.59	80.22	36.33	This work

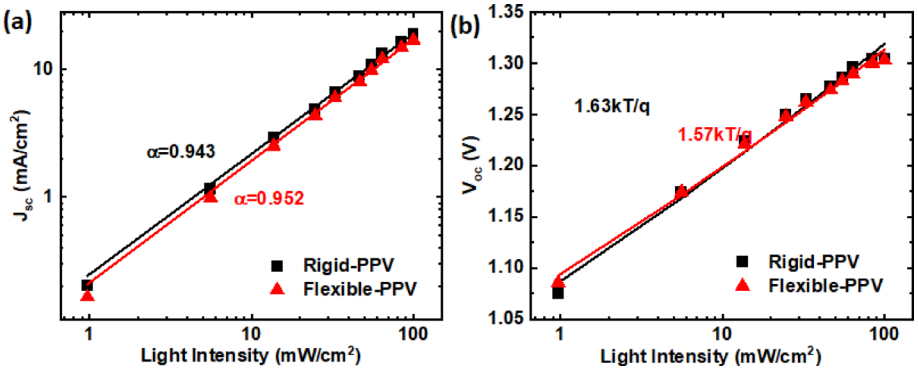

FIG. 4. (a) J_{SC} vs light intensity and (b) V_{OC} vs light intensity plots of rigid-PPV and flexible-PPV.

devices J_{EQE} were 119.47 and 125.82 μA/cm^2, respectively, under 5% for comparison with both device's corresponding J_{SC}. Figures 3(c) and 3(d) show EQE spectra and integrated J_{EQE} for 1000 lux. The flexible-PPV devices delivered similar V_{OC} to rigid-PPV while measuring them under indoor light. Furthermore, the flexible-PPV devices achieved higher V_{OC} than reported in the literature (for flexible devices), and their comparisons are summarized in Table III. The high bandgap (1.76 eV) perovskite material contributes to achieving high V_{OC}. The steady-state current density measurements show stable photocurrent under continuous illumination (1000 lux) up to 180 s, as shown in Fig. S5 (supplementary material).

The light-dependent V_{OC} and J_{SC} were measured under different light intensities (100–1 mW/cm^2), achieved using a series of neutral density filters. The recombination parameter (α) for rigid-PPV and flexible-PPV devices was calculated according to $J_{SC} \propto I_{light}^{\alpha}$, where I_{light} is incident light intensity, and the fitted plot is shown in Fig. 4(a).[22] The values of α were 0.952 and 0.943 for flexible-PPV and rigid-PPV devices, respectively. Both devices' α values imply the presence of bimolecular recombination at short-circuit current.[6] Figure 4(b) shows a light intensity-dependent V_{OC} plot, and the slope (KT/q) is calculated using a fitted curve accordingly $V_{OC} = \frac{nKT}{q} I_{light}$, where n, k_B, T, and q are the ideality factor, Boltzmann constant, temperature (in Kelvin), and elementary charge, respectively.[23] The slope deviation from 1 KT/q shows trap-assisted recombination at open circuit condition.[24] Flexible and rigid-PPV devices showed the slopes of 1.63 KT/q and 1.57 KT/q [Fig. 4(b)], respectively, suggesting that trap-assisted recombination was present in both types of devices.

In conclusion, we studied wide bandgap PPV for indoor application using dual-cation and mixed halide $[FA_{0.8}Cs_{0.2}Pb(I_{0.62}Br_{0.38})_3]$ perovskite film-based devices fabricated on flexible and rigid substrates. Under AM1.5G (1 Sun) irradiation, the flexible-PPV and rigid-PPV delivered PCE of 17.02% and 18.90%, respectively. The flexible-PPV showed lower PCE mainly due to lower J_{SC}, which was attributed to the lower optical transmission of the flexible substrate. Flexible-PPV and rigid-PPV devices showed PCE of 36.33% and 37.25%, respectively, under 1000 lux LED light illumination. Interestingly, both flexible-PPV and rigid-PPV devices delivered V_{OC} up to ∼1.11 under indoor light (1000 lux). Notably, the flexible-PPV devices showed high V_{OC} under low light. The light-dependent open-circuit voltage and short-circuit current density analysis suggested similar trap-assisted recombination (α) for both devices. The high V_{OC} of flexible-PPV devices can help to provide a low number of cell connections in series to generate the required voltage for powering IOT devices.

See the supplementary material for the device fabrication procedure, optical properties of the perovskite layer, and supporting data tables.

R.D. and W.C.T. sincerely acknowledge the ATIP (EP/T028513/1) grant for providing financial support. L.L. and H.T. acknowledge the financial support by the National Natural Science Foundation of China (U21A2076, 62305150, 52427803, and 62474086) and the Natural Science Foundation of Jiangsu Province (BK20232022, BE2022021, and BE2022026).

AUTHOR DECLARATIONS

Conflict of Interest

The authors have no conflicts to disclose.

Author Contributions

Ram Datt and Jinyan Guo contributed equally to this work.

Ram Datt: Conceptualization (lead); Data curation (equal); Formal analysis (lead); Investigation (lead); Methodology (equal); Validation (equal); Writing – original draft (lead); Writing – review & editing (lead). **Jinyan Guo:** Data curation (equal); Investigation (equal); Methodology (equal); Visualization (equal); Writing – review & editing (equal). **Renxing Lin:** Data curation (supporting); Formal analysis (supporting); Resources (supporting). **Ludong Li:** Formal analysis (equal); Funding acquisition (equal); Investigation (equal); Methodology (equal); Project administration (equal); Resources (equal); Supervision (equal); Writing – review & editing (equal). **Hairen Tan:** Funding acquisition (supporting); Investigation (supporting); Project administration (supporting); Resources (supporting); Supervision (supporting). **Wing Chung Tsoi:** Conceptualization (equal); Funding acquisition (lead); Project administration (lead); Resources (equal); Supervision (lead); Validation (equal); Writing – review & editing (equal).

DATA AVAILABILITY

The data that support the findings of the study are available within the article and its supplementary material.

REFERENCES

[1]X. Hou, Y. Wang, H. K. H. Lee, R. Datt, N. Uslar Miano, D. Yan, M. Li, F. Zhu, B. Hou, W. C. Tsoi, and Z. Li, "Indoor application of emerging photovoltaics—Progress, challenges and perspectives," J. Mater. Chem. A **8**(41), 21503–21525 (2020).

[2]I. Mathews, S. N. Kantareddy, T. Buonassisi, and I. M. Peters, "Technology and market perspective for indoor photovoltaic cells," Joule **3**(6), 1415–1426 (2019).

[3]M. Miah, M. U. Khandaker, M. Rahman, M. Nur-E-Alam, and M. A. Islam, "Band gap tuning of perovskite solar cells for enhancing the efficiency and stability: Issues and prospects," RSC Adv. **14**(23), 15876–15906 (2024).

[4]L. Li, Y. Wang, X. Wang, R. Lin, X. Luo, Z. Liu, K. Zhou, S. Xiong, Q. Bao, G. Chen, Y. Tian, Y. Deng, K. Xiao, J. Wu, M. I. Saidaminov, H. Lin, C.-Q. Ma, Z. Zhao, Y. Wu, L. Zhang, and H. Tan, "Flexible all-perovskite tandem solar cells approaching 25% efficiency with molecule-bridged hole-selective contact," Nat. Energy **7**(8), 708–717 (2022).

[5]D. Beynon, E. Parvazian, K. Hooper, J. McGettrick, R. Patidar, T. Dunlop, Z. Wei, P. Davies, R. Garcia-Rodriguez, M. Carnie, M. Davies, and T. Watson, "All-printed roll-to-roll perovskite photovoltaics enabled by solution-processed carbon electrode," Adv. Mater. **35**(16), 2208561 (2023).

[6]R. Datt, P. Caprioglio, S. Choudhary, W. Lan, H. Snaith, and W. C. Tsoi, "Engineered charge transport layers for improving indoor perovskite photovoltaic performance," J. Phys. Energy **6**(2), 025014 (2024).

[7]Y. Zheng, Y. Li, R. Zhuang, X. Wu, C. Tian, A. Sun, C. Chen, Y. Guo, Y. Hua, K. Meng, K. Wu, and C.-C. Chen, "Towards 26% efficiency in inverted perovskite solar cells via interfacial flipped band bending and suppressed deep-level traps," Energy Environ. Sci. **17**(3), 1153–1162 (2024).

[8]Z.-E. Shi, T.-H. Cheng, C.-Y. Lung, C.-W. Lin, C.-L. Wang, B.-H. Jiang, Y.-S. Hsiao, and C.-P. Chen, "Achieving over 42% indoor efficiency in wide-bandgap perovskite solar cells through optimized interfacial passivation and carrier transport," Chem. Eng. J. **498**, 155512 (2024).

[9]H. Pan, H. Shao, X. L. Zhang, Y. Shen, and M. Wang, "Interface engineering for high-efficiency perovskite solar cells," J. Appl. Phys. **129**(13), 130904 (2021).

[10]Q. Ma, Y. Wang, L. Liu, P. Yang, W. He, X. Zhang, J. Zheng, M. Ma, M. Wan, Y. Yang, C. Zhang, T. Mahmoudi, S. Wu, C. Liu, Y.-B. Hahn, and Y. Mai, "One-step dual-additive passivated wide-bandgap perovskites to realize 44.72%-efficient indoor photovoltaics," Energy Environ. Sci. **17**(5), 1637–1644 (2024).

[11]B. Orwat, Z. Shi, C. Ma, K. Jankowska, J. Nawrocik, A. Singh, Y. Zheng, W. Tu, Z. Ling, P. Dąbczyński, M. Rogala, P. Krukowski, P. J. Kowalczyk, P. Data, B. Łuszczyńska, I. Kownacki, and C. Chen, "Highly efficient indoor perovskite solar cells with 40% efficiency using perylene diimide-based zwitterionic cathode interlayers," Small **21**, 2411623 (2025).

[12]Z. Guo, A. K. Jena, and T. Miyasaka, "Halide perovskites for indoor photovoltaics: The next possibility," ACS Energy Lett. **8**(1), 90–95 (2023).

[13]R. Cheng, C. Chung, H. Zhang, F. Liu, W. Wang, Z. Zhou, S. Wang, A. B. Djurišić, and S. Feng, "Tailoring triple-anion perovskite material for indoor light harvesting with restrained halide segregation and record high efficiency beyond 36%," Adv. Energy Mater. **9**(38), 1901980 (2019).

[14]C. Zhang, C. Liu, Y. Gao, S. Zhu, F. Chen, B. Huang, Y. Xie, Y. Liu, M. Ma, Z. Wang, S. Wu, R. E. I. Schropp, and Y. Mai, "Br vacancy defects healed perovskite indoor photovoltaic modules with certified power conversion efficiency exceeding 36%," Adv. Sci. **9**(33), 2204138 (2022).

[15]M. Ma, Y. Zeng, Y. Yang, C. Zhang, Y. Ma, S. Wu, C. Liu, and Y. Mai, "Dendrimer modification strategy based on the understanding of the photovoltaic mechanism of a perovskite device under full sun and indoor light," ACS Appl. Mater. Interfaces **15**(21), 25550–25557 (2023).

[16]R. Singh, M. Parashar, S. Sandhu, K. Yoo, and J.-J. Lee, "The effects of crystal structure on the photovoltaic performance of perovskite solar cells under ambient indoor illumination," Sol. Energy **220**, 43–50 (2021).

[17]Y. Li, T. Nie, X. Ren, Y. Wu, J. Zhang, P. Zhao, Y. Yao, Y. Liu, J. Feng, K. Zhao, W. Zhang, and S. Liu, "In situ formation of 2D perovskite seeding for record-efficiency indoor perovskite photovoltaic devices," Adv. Mater. **36**(1), 2306870 (2024).

[18]Z. Skafi, J. Xu, V. Mottaghitalab, L. Mivehi, B. Taheri, F. Jafarzadeh, S. K. Podapangi, D. Altamura, M. R. Guascito, L. Barba, C. Giannini, A. Rizzo, F. De Rossi, H. Javanbakht Lomeri, L. Sorbello, F. Matteocci, F. Brunetti, and T. M. Brown, "Highly efficient flexible perovskite solar cells on polyethylene terephthalate films via dual halide and low-dimensional interface engineering for indoor photovoltaics," Sol. RRL **7**(20), 2300324 (2023).

[19]C. Liu, T. Yang, W. Cai, Y. Wang, X. Chen, S. Wang, W. Huang, Y. Du, N. Wu, Z. Wang, Y. Yang, J. Feng, T. Niu, Z. Ding, and K. Zhao, "Flexible indoor perovskite solar cells by in situ bottom-up crystallization modulation and interfacial passivation," Adv. Mater. **36**(24), 2311562 (2024).

[20]C. Teixeira, R. Fuentes-Pineda, L. Andrade, A. Mendes, and D. Forgács, "Fabrication of low-cost and flexible perovskite solar cells by slot-die coating for indoor applications," Mater. Adv. **4**(17), 3863–3873 (2023).

[21]S. Kim, H. Oh, G. Kang, I. K. Han, I. Jeong, and M. Park, "High-power and flexible indoor solar cells via controlled growth of perovskite using a greener anti-solvent," ACS Appl. Energy Mater. **3**(7), 6995–7003 (2020).

[22]R. Datt, H. K. H. Lee, M. Spence, M. Carnie, and W. C. Tsoi, "High performance non-fullerene organic photovoltaics under implant light illumination region," Appl. Phys. Lett. **122**(14), 143906 (2023).

[23]C. Liu, J. Tu, X. Hu, Z. Huang, X. Meng, J. Yang, X. Duan, L. Tan, Z. Li, and Y. Chen, "Enhanced hole transportation for inverted tin-based perovskite solar cells with high performance and stability," Adv. Funct. Mater. **29**(18), 1808059 (2019).

[24]M. Zhang, Q. Chen, R. Xue, Y. Zhan, C. Wang, J. Lai, J. Yang, H. Lin, J. Yao, Y. Li, L. Chen, and Y. Li, "Reconfiguration of interfacial energy band structure for high-performance inverted structure perovskite solar cells," Nat. Commun. **10**(1), 4593 (2019).